Theoretical Estimation of the Activation Energy for the Reaction $HO^{\bullet} + H_2O \rightarrow H_2O + {}^{\bullet}OH$: Importance of Tunneling

Michael R. Hand, Christopher F. Rodriquez, and Ian H. Williams*

Department of Chemistry, University of Bath, Bath BA2 7AY, U.K.

Gabriel G. Balint-Kurti

School of Chemistry, University of Bristol, Bristol BS8 1TS, U.K.

Received: January 22, 1998; In Final Form: April 27, 1998

Ab initio calculations for the potential barrier height for the symmetric H-atom exchange reaction $HO^{\bullet} + H_2O \rightarrow H_2O + {}^{\bullet}OH$ are reported. A value of 42.2 kJ mol^{-1} is found using the QCISD(T)/6-311+G(3df,2p) method. Multireference CISD calculations converge toward a similar value for the barrier provided that a Davidson correction is applied. The effect of quantum mechanical tunneling is investigated. Rate constants calculated by using conventional and small-curvature tunneling-corrected transition state theory with the UMP2/6-311G(d,p) transition structure and reaction path are compared for a wide range of temperatures. Tunneling reduces the Arrhenius activation energy, obtained from the temperature dependence of the calculated rate constants, by at least 20 kJ mol^{-1} at 300 K. The best theoretical estimate for the Arrhenius activation energy at 300 K is 21.2 kJ mol^{-1}; the discrepancy between this and the experimental value of 17.6 ± 2 kJ mol^{-1} is likely to be due to neglect of large-curvature tunneling effects. The QCISD(T)/6-311+G(3df,2p) calculated enthalpy of association of $HO^{\bullet} + H_2O \rightarrow HO^{\bullet}\cdots HOH$, the hydrogen-bonded precursor complex, is −8.9 kJ mol^{-1}. The best theoretical estimate for the intrinsic barrier height for the symmetric H-atom exchange $HO^{\bullet}\cdots HOH \rightarrow HOH\cdots{}^{\bullet}OH$ is 25.1 kJ mol^{-1}.

Introduction

The degenerate hydrogen atom transfer between a hydroxyl radical and water molecule,

$$HO^{\bullet} + HOH \rightarrow HOH + {}^{\bullet}OH \qquad (1)$$

is a ubiquitous, but kinetically silent, reaction which serves as a prototype for H atom abstractions involving $^{\bullet}$OH; such processes have a primary role in the breakdown of many organic molecules in the troposphere.[1]

In an earlier theoretical study[2] we calculated the barrier height for reaction 1 using various established molecular orbital (MO) methods and standard basis sets. The unrestricted Hartree−Fock (UHF) method gave very high barriers, but inclusion of more electron correlation diminished the barrier considerably: with basis sets of modest size, similar barrier heights were obtained by using both second-order spin-projected Møller−Plesset perturbation theory (PUMP2)[3] and quadratic configuration interaction [QCISD(T)].[4] A final prediction for the activation enthalpy was obtained by several stages. First, a Boys−Bernardi counterpoise correction[5] for basis-set superposition error (BSSE) was applied to the PUMP2/6-311++G(3d,2p) energy. Then, to account for better electron correlation in the QCISD(T) method, an increment equal to the difference between the QCISD(T) and PUMP2/6-311+G** barrier heights was added. Each of the correlation-energy corrections was scaled in the manner proposed by Truong and Truhlar.[6] Finally, a correction for the difference in thermal vibrational energy between reactants and transition state was made, resulting in an estimated activation enthalpy of 44 kJ mol^{-1}. In the absence of an experimental Arrhenius activation energy for reaction 1, an empirical estimate of 22 ± 4 kJ mol^{-1} for the activation enthalpy was made by using the Marcus relation.

One possible reason for the discrepancy between the calculated and empirical activation enthalpy estimates was recognized to be quantum mechanical tunneling, which is often significant in H atom transfers. Isotopic substitution experiments demonstrate the importance of tunneling in these reactions: the ratio of the rate constants for protium and deuterium transfer can exceed by several orders of magnitude the value predicted from just vibrational zero-point energy differences.[7] The effect of tunneling on activation energies is not obvious. Due to quantum tunneling, the probability for transmission through the reaction barrier is greater than zero at energies below the classical threshold, and the rate constant is increased. At low temperatures the translational energy is mostly less than the classical threshold, so the reaction proceeds mainly by tunneling, and the increase in rate constant is greater than at high temperature. There is therefore an upward curvature in an Arrhenius plot as the temperature decreases, and the activation energy is lowered at low temperatures.

A comprehensive treatment of tunneling in a chemical reaction requires a quantum mechanical calculation of the nuclear motion, for a thermal distribution of translational and internal energies. This very difficult task has been accomplished only for a few elementary reactions.[8] To calculate nuclear motion in a quasi-classical trajectory (QCT) model is more straightforward, but this omits tunneling. Where comparison has been made, thermal rate constants from classical trajectory calculations have not been found to differ greatly from quantum

* Corresponding author. E-mail: i.h.williams@bath.ac.uk.

S1089-5639(98)00838-X CCC: $15.00
Published on Web 06/29/1998

mechanical values, even over the temperature range where tunneling is important. However, this result actually arises because of a problem with the incorporation of zero-point vibrational energy in the classical trajectory calculations: since no restraint can be made on the redistribution of energy in classical mechanics, the initial zero-point energy used in QCT calculations assists in crossing the barrier and artificially increases the rate of reaction.

Full classical trajectory studies are still large calculations, and in view of their drawbacks transition state theory (TST) presents an attractive alternative.[9] The absolute rate constant in TST is given by

$$k^{\mathrm{TST}} = \sigma\,(k_{\mathrm{B}}T/h)\,[Q^{\ddagger}(T)/Q^{\mathrm{R}}(T)]\exp(-E_0/k_{\mathrm{B}}T) \qquad (2)$$

The only unknown quantities needed to apply this equation are the partition functions for the reactants and the transition state, $Q^{\mathrm{R}}(T)$ and $Q^{\ddagger}(T)$, and the height of the reaction barrier, E_0. It is successful for systems obeying the fundamental TST assumption that trajectories do not recross the dividing surface between reactants and products. In TST the dividing surface passes through the saddle point at the top of the reaction barrier, whereas in variational TST (VTST) the rate of reaction is minimized by placing the dividing surface in the position that minimizes the amount of recrossing; the transition state is thus redefined as the point of maximum free energy on the reaction path.[10]

Tunneling may be included in TST by calculating the motion along the reaction path quantum mechanically. This may be done by using a simple model for the reaction barrier, as in the Wigner[11] or Eckart[12] corrections, but with semiclassical methods the actual reaction-path barrier may be used.[13] The one-dimensional model of quantum dynamics produced by this type of calculation is often not sufficient, and the multidimensional nature of the reaction path must be considered. An energy contour plot for atom transfer, if plotted in the conventional manner as a function of those coordinates which eliminate cross-terms in the kinetic energy expression, is V-shaped: crossing the barrier from the reactant valley to the product valley requires a turn through an acute angle.[14] Quantum wave packet calculations for model surfaces have demonstrated that the quantum flux prefers to cut the corner of the V rather than follow the reaction path.[15] This involves a higher barrier than at the saddle point but a decreased tunneling distance. With several methods developed to account for reaction path curvature, rate constants agreeing with exact results[16] have been calculated by using variational and conventional TST.[17] We now report the results of rate constant calculations for reaction 1 including the effects of tunneling and reaction path curvature on an ab initio potential energy surface.

It is important to note the distinction between a potential energy barrier and an activation energy, particularly for a reaction in which tunneling may play an important role. The Arrhenius activation energy is obtained empirically from the temperature dependence of the observed rate coefficient:[18]

$$E_{\mathrm{a}} = RT^2\,\mathrm{d}(\ln k)/\mathrm{d}T \qquad (3)$$

For a bimolecular reaction in the (ideal) gas phase, the activation energy is related to the activation enthalpy by[18]

$$E_{\mathrm{a}} = \Delta H^{\ddagger} + RT - \Delta n^{\ddagger}RT = \Delta H^{\ddagger} + 2RT \qquad (4)$$

If the activation enthalpy is dominated by the structural properties of the transition state as a molecular "substance", it has a physical meaning as an energy barrier to reaction. However, if the temperature dependence of the observed rate coefficient is determined to a large extent by tunneling, which induces strong non-Arrhenius behavior, then although a formal Arrhenius activation energy (or activation enthalpy) is obtained over a limited temperature range it no longer has a clear physical interpretation as an energy barrier: the activation energy has a large "nonsubstantial" contribution from the dynamics and the properties of the potential-energy surface rather than from the transition-state structure itself.[17]

In our earlier work,[2] the largest basis set used with the PUMP method was 6-311++G(3d,2p), while calculations made by using the complete-active-space self-consistent field (CASSCF) and multireference configuration interaction (MRCISD) methods were restricted to the 6-31G(d) basis. Barrier heights found using these variational methods were consistently higher than those with the PUMP and QCISD(T) methods. To investigate this discrepancy, we have now made further calculations at the MRCISD level using basis sets as large as those used previously with the PUMP method. In addition we have now used the G2 protocol,[19] based on a QCISD(T) energy with basis-set corrections evaluated by the UMP method.

Methods

(i) Semiclassical Variational Transition State Theory (VTST). The POLYRATE program[20] was used to calculate temperature-dependent rate constants with semiclassical VTST. The minimum-energy path (MEP) required in these calculations was computed by using the intrinsic reaction coordinate (IRC) algorithm[21] in the GAUSSIAN92 program.[22] The MEP was followed in mass-weighted internal coordinates using a step length of 0.1 bohr amu$^{1/2}$, where the mass-weighting uniformly makes the mass 1.0 amu. The UMP2/6-311G(d,p) method was chosen for use in these calculations, since the potential energy barrier height of 45.0 kJ mol^{-1} obtained at this level is in agreement with that calculated by using the more expensive methods [e.g., QCISD(T)/6-311++G(3d,2p), see below], and the second derivative matrix could be calculated at each point on the reaction path.

Quantum tunneling is put into classical TST via a correction factor, κ, defined by

$$\kappa(T) = \frac{\int_0^{\infty} P_Q(E)e^{-E/k_{\mathrm{B}}T}\,\mathrm{d}E}{\int_{E_0}^{\infty} P_C(E)e^{-E/k_{\mathrm{B}}T}\,\mathrm{d}E} \qquad (5)$$

In this equation $P_{\mathrm{Q}}(E)$ is the quantum transmission probability for the barrier as a function of translational energy, and $P_{\mathrm{C}}(E)$ is its classical equivalent. $P_{\mathrm{C}}(E)$ is assumed to be a step function, rising from zero to unity at the threshold energy E_0, which is correct if there is no coupling between barrier crossing and internal coordinate motion. Integrating the denominator in eq 5 leads to

$$\kappa(T) = \frac{\exp[E_0/k_{\mathrm{B}}T]}{k_{\mathrm{B}}T}\int_0^{\infty} P_Q(E)e^{-E/k_{\mathrm{B}}T}\,\mathrm{d}E \qquad (6)$$

Tunneling is important at low temperatures, where practically all molecules lie in their vibrational ground states. Therefore, to calculate the quantum transmission probability $P_{\mathrm{Q}}(E)$, the reactants are put in their ground vibrational states. It is also assumed that throughout the reaction the system remains in its vibrational ground state (vibrational adiabaticity), since tunneling directly into vibrationally excited states of the products is

unimportant in the thermoneutral reaction 1. The adiabatic energy at each point on the MEP is obtained by adding to the potential energy the sum of the zero-point energies for the vibrational modes orthogonal to the MEP.

The VTST/MEPSAG (variational TST/minimum-energy path semiclassical adiabatic ground state)[17] method calculates tunneling-corrected reaction rate constants directly along the one-dimensional reaction path energy profile. However, quantum mechanical calculations of reaction dynamics show that the quantum flux does not keep to the reaction path but cuts the corner, reducing the tunneling distance and increasing the reaction probability. The SCSAG (small curvature semiclassical adiabatic ground state)[17] method takes account of the curvature of the reaction path discussed above: this method follows an alternative reaction path, shorter than the MEP, namely, the locus of vibrational turning points on the concave side of the curve. The mass for motion along the MEP is now varied according to the curvature of the path. Where the reaction path is acutely curved, as in the transfer of a hydrogen atom between two heavy fragments, the SCSAG method provides an inadequate account of the tunneling. In this case the quantum transmission probability can be calculated by using straight paths to connect turning points on the MEP in the entrance and exit valleys, which requires that the PES on the ridge separating the entrance and exit valleys is known; however, this information is not obtainable from the reaction-path representation of an ab initio PES alone, and so we have not calculated large-curvature tunneling corrections directly in this work. Instead, to estimate the likely effect on the activation energy of including large curvature tunneling, we compared reaction 1 with other H atom transfer reactions that have similar reaction path curvatures.

Arrhenius activation energies were obtained from the calculated rate constants as the slopes of plots of ln k against $1/T$ over a series of limited temperature ranges.

(ii) Ab Initio Barrier Height Calculations. The CASSCF and internally contracted MRCISD calculations in this work were performed by using the MOLPRO program.[23] The full-valence active space used in the CASSCF calculations comprised the molecular orbitals and electrons that derive from the valence shell of each atom. For the transition state this procedure gave an active space of 15 electrons in 11 orbitals. The configurations used in the CASSCF wave function were then used to provide the reference functions for an MRCISD calculation. The number of configurations included as references in the MRCISD calculations was selected by using a threshold value for the coefficient of the configuration function in the CASSCF wave function. The MRCISD calculations included single and double excitations of all valence electrons to all virtual orbitals. To correct for the lack of size consistency in this approach,[24] barrier heights were calculated by reference to the energy of a supermolecule containing the $HO^{\bullet}$ and H_2O fragments separated by 1000 Å. An estimate of the effect of higher excitations was made by applying the multireference Davidson correction[25] to the MRCISD total energies.

In our earlier work, the difference between the BSSE-corrected, correlation-scaled QCISD(T)/6-311+G(d,p) and PUMP2/6-311+G(d,p) barriers was added to the BSSE-corrected, correlation-scaled PUMP2/6-311++G(3d,2p) value in order to evaluate a "best" estimate for the barrier height.[2] This allowed a separation of improvements in basis set from any improvements in electron correlation. In the G2 protocol[19] the same separation is made, but the QCISD(T)/6-311G(d,p) energy is the starting point, and the basis-set correction added is the difference between UMP4/6-311+G(3df,2p) and UMP4/6-311G(d,p) energies (without BSSE or correlation-energy scaling corrections). UMP2/6-31G(d) geometries are used in these calculations, and the zero-point vibrational energy evaluated at the HF/6-31G(d) level is added. An additional isogyric correction would be applied if there were a change in the number of unpaired electrons. This method has been demonstrated to give heats of reaction accurate to within 4 kJ mol^{-1} for molecules containing first-row atoms[19] and 6 kJ mol^{-1} for transition structures.[26] To provide a cross-check of our other calculations, we have applied the G2 protocol to reaction 1 using GAUSSIAN92. Since there is no change in the number of unpaired electrons on going to the transition state for this reaction, there is no isogyric correction.

Association of $HO^{\bullet}$ and H_2O to form hydrogen-bonded complexes was investigated by means of calculations performed using the GAUSSIAN94 program,[27] including evaluation of BSSE corrections.

Results and Discussion

(i) Minimum Energy Reaction Path. In Table 1 are geometries for the reactants and the transition state of the exchange reaction (1) calculated by using the UMP2 method with the 6-31G(d) and 6-311G(d,p) bases. In our previous study for this reaction,[2] the transition state geometry obtained with both the UHF and CASSCF methods had C_2 symmetry. However, vibrational frequencies calculated for the C_2-symmetric structure (Figure 1, denoted $HOHOH^{\bullet}$) found by using the UMP2 method, shown in Table 1, reveal that in this case it is an energy minimum rather than a saddle point, since there is no vibrational mode with an imaginary frequency. A true saddle point was found on each of the UMP2 potential energy surfaces at an asymmetric geometry (denoted $HOHOH^{\bullet\ddagger}$) with the central O···H distances being one slightly longer and one slightly shorter than at the C_2 minimum. The energies of the fragments and of both the symmetric $HOHOH^{\bullet}$ and asymmetric $HOHOH^{\bullet\ddagger}$ systems are given in Table 1 for two different basis sets using the UMP2 method. Fortunately, since the difference in energy in the UMP2/6-311G(d,p) method between this saddle point and the symmetric minimum is only 0.34 kJ mol^{-1}, *the depression at the top of the barrier is unimportant in comparison to its total height of 45.0 kJ* mol^{-1}. A similar effect has been observed in a study[28] of the isoelectronic reaction $F^{\bullet}$ + HF, in which there is an avoided-crossing between an electronic state corresponding to bond breaking and formation and two broken-symmetry states for hydrogen-bonded species. In calculations using the MP2 method there is an abrupt jump from one state to the other at the avoided-crossing, and as a result there is an energy maximum at a short distance from the symmetric structure. However, when the QCISD(T) and coupled clusters (CCSD) methods are used the saddle point is found to be at its expected symmetric position.[28]

The reaction path used in the POLYRATE calculations was computed by starting from the asymmetric saddle point at the lip of the shallow basin on top of the barrier. It was assumed that this path would differ only slightly from the path that would have been obtained by starting from the correct symmetric saddle point. To include the symmetric point in the POLYRATE path it was converted to a saddle point by making negative the eigenvalue for what should have been the transition vector, and then recalculating the second derivative matrix using the eigenvectors and (modified) eigenvalues. The symmetric point was made into the maximum on the reaction path by adding twice the energy difference between it and the nonsymmetric saddle point, and it was made into the origin of the reaction

TABLE 1: Optimized Geometries (Bond Lengths, Å; Angles, deg), Vibrational Frequencies (expressed as wavenumbers, cm^{-1}), Total Energies (hartree), Zero-Point Energies (kJ mol^{-1}) of Species along Reaction Path for HO• + H_2O Hydrogen Atom Transfer, and Barrier Height (kJ mol^{-1})

species		UMP2(fc)/6-31G(d)	UMP2(fu)/6-311G(d,p)
HO•			
	O−H	0.979	0.966
	frequencies	3740	3858
	ZPE	22.37	23.08
	total energy	−75.521 03	−75.572 90
H_2O			
	O−H	0.969	0.957
	H−O−H	104.1	102.5
	frequencies	1735, 3773, 3915	1668, 3909, 4017
	ZPE	56.36	57.38
	total energy	−76.196 85	−76.263 97
HOHOH• (C_2)			
	O···H	1.156	1.139
	O−H	0.977	0.964
	O···H···O	136.4	140.1
	H···O−H	103.2	102.0
	dihedral O···H···O−H	61.4	59.1
	frequencies	403, 493, 624, 1005, 1404, 1572, 1795, 3757, 3762	386, 504, 619, 970, 1352, 1734, 1891, 3882, 3885
	ZPE	88.61	91.05
	total energy	−151.699 14	−151.819 77
HOHOH•‡ (C_1)			
	O···H	1.188	1.179
	O'···H	1.132	1.109
	frequencies	1582*i*, 406, 494, 617, 1109, 1493, 1780, 3757, 3765	1814*i*, 394, 501, 624, 1053, 1421, 1734, 3880, 3887
	ZPE	80.40	80.71
	total energy	−151.699 08	−151.819 64
barrier height		49.4	45.0

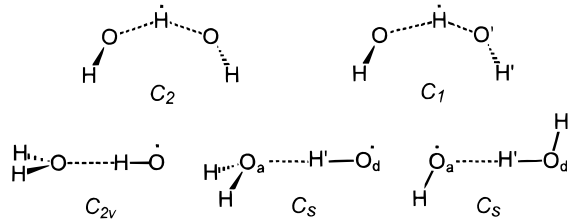

Figure 1. Schematic H_3O_2 complexes.

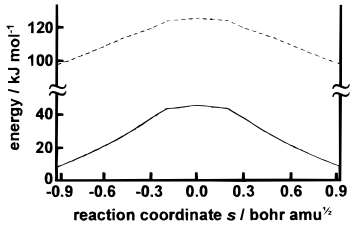

Figure 2. Potential energy (solid line) and adiabatic ground-state potential (dashed line) along the minimum energy reaction path.

coordinate by adding to the reaction coordinate of each point the distance along the IRC between the symmetric point and the nonsymmetric saddle point. The two nonsymmetric saddle points on either side of the redefined origin were not included in the path, since their second derivative matrixes would have been inconsistent with the changes made to the symmetric point. The modifications made to the UMP2 reaction path involved altering the coordinates and second derivative matrixes of only the starting point of the path; these alterations were very small as compared to changes occurring between the first two points of the reaction path.

A plot of the UMP2/6-311G(d,p) MEP used in the POLYRATE calculations is shown in Figure 2, in which the origin of energy corresponds to far-separated HO• and H_2O species. Also shown in Figure 2 is the adiabatic ground-state energy, $V^G_a(s)$, obtained by adding to the MEP potential the zero-point energy for the vibrational modes orthogonal to the reaction coordinate. $V^G_a(s)$ tracks closely the change in $V(s)$ as s is varied, indicating that the zero-point energy does not vary much along the reaction path. Inspection of the results in Table 1 shows that the UMP2/6-311G(d,p) zero-point energy increases by only 0.25 kJ mol^{-1} between the reactant and transition state geometries. Although the frequency of the vibrational mode that correlates with the symmetric stretch of H_2O drops from 3909 to 1734 cm^{-1} at the transition state, the creation of four additional vibrational modes leaves the overall zero-point energy almost unchanged.

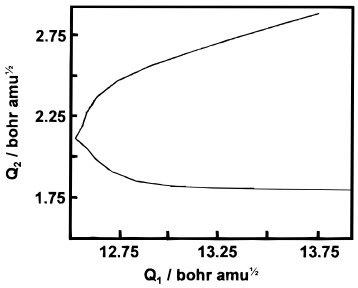

Figure 3. Minimum energy path plotted in the skewed mass-scaled coordinates (as defined in ref 14, pp 165−167): $Q_1 = pD(O_aH\cdots H'O_dH)$ and $Q_2 = pD(H'\cdots O_dH) \times \sin\beta$, where $p = [m_{OH}(m_H + m_{OH})/(m_{HOHOH})]^{1/2}$, D is a distance between the centers of mass of the fragments indicated in parentheses, and the angle β is as given by eq 7.

A further two-dimensional representation of the reaction path is shown in Figure 3. In this plot Q_1 and Q_2 are the mass-scaled coordinates corresponding, respectively, to the distance between the center of mass of HO• and the center of mass of H_2O and to the distance between the transferring H atom and the center of mass of •OH. The angle between the exit and entrance channels is given by eq 7 below;[14] evaluation of this expression gives $\beta = 19°$.

$$\cos^2\beta = \frac{m_{OH}m_{OH}}{(m_{OH} + m_H)(m_H + m_{OH})} \qquad (7)$$

TABLE 2: Rate Constants for $HO^{\bullet} + H_2O$ Hydrogen Atom Transfer Calculated by Using Transition State Theory with Various Quantum Corrections

temperature, K	rate constant, cm^3 $molecule^{-1}$ s^{-1}		
	VTST[a]	VTST/MEPSAG[b]	VTST/SCSAG[c]
300	1.349×10^{-20}	5.499×10^{-20}	6.726×10^{-19}
350	1.585×10^{-19}	4.179×10^{-19}	2.446×10^{-18}
400	1.022×10^{-18}	2.082×10^{-18}	7.805×10^{-18}
450	4.432×10^{-18}	7.643×10^{-18}	2.131×10^{-17}
500	1.458×10^{-17}	2.244×10^{-17}	5.085×10^{-17}
550	3.930×10^{-17}	5.570×10^{-17}	1.085×10^{-16}
600	9.104×10^{-17}	1.216×10^{-16}	2.116×10^{-16}
650	1.880×10^{-16}	2.398×10^{-16}	3.827×10^{-16}
700	3.546×10^{-16}	4.363×10^{-16}	6.506×10^{-16}
800	1.027×10^{-15}	1.200×10^{-15}	1.622×10^{-15}
900	2.435×10^{-15}	2.747×10^{-15}	3.478×10^{-15}
1000	5.007×10^{-15}	5.511×10^{-15}	6.664×10^{-15}

[a] Variational transition state theory (VTST) (see ref 17). [b] Minimum energy path semiclassical adiabatic ground state (MEPSAG, see ref 17). [c] Small curvature path semiclassical adiabatic ground state (SCSAG, see ref 17).

The artificial energy minimum found at the top of the barrier in the UMP2 method is manifested in this plot as the protrusion at the origin of the reaction path.

(ii) Tunneling Effects. The UMP2/6-311G(d,p) MEP in Figure 2 for reaction 1 was used in conjunction with the POLYRATE computer code[20] to calculate the rate constants in Table 2, from which the Arrhenius activation energies and preexponential factors shown in Table 3 were derived. Although the variational version of TST was used to generate the results presented here, locating the transition state at the saddle point gave very similar results, indicating that for this reaction the influence of trajectories recrossing the saddle point was negligible. At the lower end (300−350 K) of the range of temperatures considered, where quantum effects are more important, inclusion of tunneling along a straight reaction path (VTST/MEPSAG) produced a reduction of the activation energy from 43.0 to 35.4 kJ mol^{-1}. After making allowance for corner-cutting using the small-curvature method (VTST/SCSAG) a further reduction of E_a to 22.5 kJ mol^{-1} was found. The reduction in E_a produced in the small-curvature model may possibly be overestimated, since insufficient account might be taken in the model for the increase in barrier height encountered along a path that cuts the corner of the reaction path: it is assumed that all paths run parallel to the MEP. A noticeable feature of the results in Table 3 is that, even over a temperature range 600−650 K, tunneling still reduces E_a by 8.5 kJ mol^{-1}.

For hydrogen atom transfer between heavy species, where the reaction path turns around sharply, the large curvature method is more accurate than VTST/SCSAG. It can, however, only be used where an analytic representation of the potential energy surface for the reaction is available. The effect of including large curvature tunneling for reaction 1 can therefore only be inferred by examining the behavior found in other hydrogen transfer systems. As an indicator of the severity of reaction path curvature likely to be found in a particular system the angle β (eq 5) is used. For the three-body reaction $^{\bullet}O^{\bullet} + H_2 \rightarrow {}^{\bullet}OH + {}^{\bullet}H$, β has a value of 47°, so by comparison to reaction 1 (for which β has a value of 19°) the reaction path curvature should be much less, since the exit and entrance channels intersect at a less acute angle. At a temperature of 300 K, inclusion of small-curvature tunneling in VTST reduces E_a from 44 to 30 kJ mol^{-1}.[29] Inclusion of large-curvature tunneling produces a further reduction in E_a of 1 kJ mol^{-1}. So for this reaction, as expected, large-curvature effects are negligible. The reaction $CF_3^{\bullet} + CD_3H \rightarrow CF_3H + {}^{\bullet}CD_3$ gives a value for β of 16°, which implies that large curvature effects should be more important in this case than for reaction 1. Inclusion of small-curvature tunneling reduces E_a from 54 to 44 kJ mol^{-1} at 300 K; large-curvature tunneling produces a further reduction of 3 kJ mol^{-1}.[29] Comparing these two reactions, the overall reduction in E_a due to tunneling is greater for $^{\bullet}O^{\bullet} + H_2$ than for $CF_3^{\bullet} + CD_3H$, as the effective mass crossing the barrier is greater in the latter case, making quantum effects less important. However, the fraction of the total reduction in E_a arising from large curvature effects is, as expected, greater for $CF_3^{\bullet} + CD_3H$. It would be wrong to draw a firm conclusion from this comparison, since the behavior found in a reaction system will depend on the detailed topography of the PES. However, if it is assumed that the fractional reduction of E_a due to large-curvature effects is as great as that for $CF_3^{\bullet} + CD_3H$, then inclusion of large-curvature tunneling for reaction 1 would produce a further reduction of E_a by 5 kJ mol^{-1}, which would bring it down to 17.5 kJ mol^{-1} at 300 K.

(iii) The Role of the Encounter Complex $HO^{\bullet}\cdots HOH$. As noted in our previous paper, the global minimum on the $HO^{\bullet} + H_2O$ potential energy surface is a complex $H_2O\cdots HO^{\bullet}$ in which the hydroxyl radical donates a hydrogen bond to an oxygen lone pair on the water molecule;[2] the optimum geometry is not the C_{2v} symmetrical species (Figure 1) but the close-by species of C_s symmetry, as computed by Xie and Schaefer, for which the $^2A'$ state is slightly lower in energy than the $^2A''$ state.[30] However, the encounter complex relevant to hydrogen atom abstraction from molecules HOR by radicals $R'O^{\bullet}$ is not this global minimum structure but the species $HO^{\bullet}\cdots HOH$ in which the hydrogen-bond donor is the water molecule instead of the hydroxyl radical. The optimum geometry of this C_s symmetrical species (Figure 1), for which the $^2A''$ state is slightly lower in energy than the $^2A'$ state, had previously been computed by Schaefer and co-workers using a restricted CISD/DZP method.[31] Geometrical parameters for the $^2A'$ state of $H_2O\cdots HO^{\bullet}$ [optimized at the UMP2/6-31G(d) level] and for the $^2A''$ state of $HO^{\bullet}\cdots HOH$ [optimized at the UMP2/6-311++G(d,p) level] are presented in Table 4. In Table 5 are shown total energies for these complexes calculated by using the methods needed to apply the G2 protocol, together with their association energies. The row marked G2(MP2) indicates that the basis set corrections were evaluated[32] at the UMP2 level rather than UMP4, and the energies presented include vibrational zero point energy; at this level of calculation the $HO^{\bullet}\cdots HOH$ species lies 13 kJ mol^{-1} higher in energy than the global minimum species $H_2O\cdots HO^{\bullet}$.

We have studied the complex of significance as the precursor to H atom transfer, $HO^{\bullet}\cdots HOH$, at the QCISD(T)/6-311+G(3df,2p) level, which avoids the additivity assumptions of the G2 protocol, and have evaluated the zero point energy, thermal energy, and $PV = RT$ contribution to the enthalpy at 298K with the UHF/6-311++G(d,p) method, with vibrational frequencies scaled by 0.89. A remaining source of potential error is BSSE: each fragment, $HO^{\bullet}$ and HOH, is stabilized at its geometry in the hydrogen-bonded complex $HO^{\bullet}\cdots HOH$ by the nearby presence of the basis functions for the other fragment. van Lenthe and co-workers[33] have argued persuasively that the BSSE is correctly estimated by the Boys−Bernardi counterpoise procedure,[5] in which the energy of each fragment is calculated at the geometry it has in the adduct, both with and without the presence of the ghost orbitals of the other fragment. The BSSE at the QCISD(T)/6-311+G(3df,2p) level is determined by this means to be less than 2 kJ mol^{-1}. Thus, a best estimate for the

TABLE 3: Calculated Arrhenius Activation Energies (E_a, kJ Mol^{-1}) and Preexponentials (A, cm^3 Molecule^{-1} s^{-1}) for HO$^\bullet$ + H_2O Hydrogen Atom Transfer

	VTST[a]		VTST/MEPSAG[b]		VTST/SCSAG[c]	
temp range, K	E_a	A	E_a	A	E_a	A
300−350	43.010	4.2×10^{-13}	35.414	8.1×10^{-14}	22.541	5.7×10^{-15}
400−450	43.916	5.5×10^{-13}	38.931	2.5×10^{-13}	30.069	6.6×10^{-14}
500−550	45.307	7.9×10^{-13}	41.580	5.0×10^{-13}	34.677	2.1×10^{-13}
600−650	47.040	1.1×10^{-12}	44.054	8.3×10^{-13}	38.436	4.7×10^{-13}
700−800	49.505	1.8×10^{-12}	47.095	1.4×10^{-12}	42.542	9.7×10^{-13}
900−1000	53.955	3.3×10^{-12}	52.116	2.9×10^{-12}	48.650	2.3×10^{-12}

[a] Variational transition state theory (VTST) (see ref 17). [b] Minimum energy path semiclassical adiabatic ground state (MEPSAG, see ref 17). [c] Small curvature path semiclassical adiabatic ground state (SCSAG, see ref 17).

TABLE 4: Optimized Geometries and Frequencies for Hydrogen Bonded Association Complexes

coordinate	$H_2O_a\cdots H'O_d^\bullet$ (C_s) UMP2/6-31G(d)	$HO_a^\bullet\cdots H'O_dH$ (C_s) UMP2(fu)/6-311++G(d,p)
$O_a\cdots H'$	1.916	2.098
O_d-H	0.986	0.958
O_a-H	0.970	0.969
O_d-H'		0.962
H−O−H	104.7	103.9
$H'\cdots O_a-H$		109.2
$O\cdots H'-O$	170.5	160.7
dihedral $H-O\cdots H'-O$	120.7	180.0
frequencies/cm^{-1}	142, 193, 236, 519, 673, 1726, 3633, 3768, 3902	74, 113, 145, 307, 359, 1742, 4048, 4128, 4254[a]
ZPE, kJ mol^{-1}	88.48	90.79

[a] UHF/6-311++G(d,p) frequencies for HO$^\bullet\cdots$HOH.

TABLE 5: Total Energies (hartree) and Association Energies (kJ mol^{-1}) Relating to the Hydrogen Bonded Association Complexes $H_2O\cdots HO^\bullet$ and $HO^\bullet\cdots HOH$

	total energies//UMP2/6-31G(d)			ΔE_{assoc}	total energies//UMP2/6-311++G(d,p)			ΔE_{assoc}
method	H_2O	$HO^\bullet$	$H_2O\cdots HO^\bullet$	($H_2O\cdots HO^\bullet$)	H_2O	$HO^\bullet$	$HO^\bullet\cdots HOH$	($HO^\bullet\cdots HOH$)
UMP2/6-311G(d,p)	−76.263 63	−75.572 76	−151.848 60	−32.1	−76.263 94	−75.572 90	−151.843 69	−18.0
UMP2/6-311+G(3df,2p)	−76.318 10	−75.617 41	−151.945 03	−25.0	−76.318 26	−75.617 54	−151.941 56	−15.1
QCISD(T)/6-311G(d,p)	−76.276 05	−75.589 21	−151.876 88	−30.5	−76.276 31	−75.589 26	−151.872 36	−17.8
G2(MP2)[a]	−76.330 51	−75.633 86	−151.973 31	−23.5	−76.332 04	−75.634 82	−151.979 63	−15.0
QCISD(T)/6-311+G(3df,2p)					−76.331 88	−75.636 84	−151.974 60	−15.4
($E_{zp} + E_{th} + RT$)[b]					0.026 93	0.012 59	0.041 27	+4.6
QCISD(T)/6-311+G(3df,2p)[c]					−76.331 89	−75.636 85		
BSSE correction[d]					−76.332 23	−75.637 25		+1.9
ΔH_{assoc} best estimate (298 K)								−8.9

[a] Basis set additivity term evaluated with UMP2 method instead of UMP4.[32] [b] Zero point energy, thermal energy and $PV = RT$ enthalpic contributions at 298 K. [c] Energy of each distorted fragment, as in $HO^\bullet\cdots$HOH. [d] Energy of each distorted fragment, as in $HO^\bullet\cdots$HOH, in the presence of ghost orbitals of the counter-fragment.

enthalpy of association of $HO^\bullet\cdots$HOH may be obtained by summing the contributions ΔE_{assoc}[QCISD(T)/6-311+G(3df,-2p)] + $\Delta(E_{zp} + E_{th} + PV)_{298}$ + BSSE (where $PV = RT$), which yields $\Delta H_{assoc} = -8.9$ kJ mol^{-1} at 298 K.

In the absence of observed rate data and of an experimental value for the activation energy for reaction 1, in our earlier study[2] we attempted to predict a value for the activation energy using the Marcus relation:[34]

$$\Delta H^\ddagger = \Delta H^\ddagger_{int} + \Delta H_{rxn}/2 + (\Delta H_{rxn})^2/16\Delta H^\ddagger_{int} \qquad (8)$$

For a series of similar group transfer reactions this equation relates the activation enthalpy $\Delta H^\ddagger$ to the enthalpy of reaction ΔH_{rxn}. $\Delta H^\ddagger$ may be obtained from the experimental activation energy E_a using the relation $\Delta H^\ddagger = E_a - 2RT$ (cf. eq 4). The intrinsic barrier, $\Delta H^\ddagger_{int}$, is the value of $\Delta H^\ddagger$ for a thermoneutral reaction, for which $\Delta H_{rxn} = 0$. The activation energy for the symmetric reaction 1 may therefore be considered as the intrinsic barrier for a series of reactions involving hydrogen transfer between oxygen atom centers. A consistent value for $\Delta H^\ddagger_{int}$ of 22 kJ mol^{-1} was apparently found[2] by using the measured Arrhenius activation energies[35] and heats of reaction[36] of three nonsymmetric reactions ($HO^\bullet$ + HOOH → H_2O + $HO_2^\bullet$, O + H_2O → $2HO^\bullet$, O_2 + HOOH → $2HO_2^\bullet$). Since this figure did not appear to agree with the value of 44 kJ mol^{-1} calculated for the height of the reaction barrier, a possible energy reduction of the activation energy due to quantum tunneling effects was suggested.[2] The discussion in the previous section shows that there is indeed a large reduction in E_a due to tunneling for this system, and an apparent agreement with the derived Marcus intrinsic barrier. However, an important consideration that was neglected in our earlier estimation of $\Delta H^\ddagger_{int}$ was the depth of the energy well for association of $HO^\bullet$ with H_2O in the encounter complex ($HO^\bullet\cdots$HOH) and for the corresponding encounter complexes involved in the three nonsymmetric reactions. The simple form of the Marcus relation, eq 8, applies only to a single elementary step between adjacent energy minima (B···HA and BH···A in Figure 4), but in the previous work the activation energies $(\Delta H^\ddagger)^*$ and heats of reaction $(\Delta H_{rxn})^*$ were erroneously taken as between the separated reactant and product species (B + HA and BH + A in Figure 4). We note that the same mistake was made in another recent study,[37] which went on to conclude that the Marcus relation was unreliable for correlating activation energies and heats of reaction for atom transfer reactions.

Table 6 contains experimental data for the three reactions mentioned above, which involve H-atom transfer between

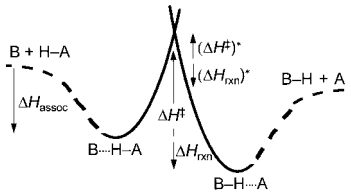

Figure 4. Enthalpies of activation and enthalpies of reaction for Marcus-theoretical treatment of atom transfer reactions: atom transfer elementary step (solid lines) and association/dissociation steps (dashed lines).

TABLE 6: Thermochemical Data Relating to Reaction Barriers for Hydrogen Atom Exchanges between Oxygen Species

reaction[a]	ΔH_{rxn}	E_a	$\Delta H^{\ddagger}$ (expt)[b]	$\Delta H^{\ddagger}$ (predicted)[c]
$HO^{\bullet} + HOOH \rightarrow H_2O + HO_2^{\bullet}$	−132.2	7.5	11.5	8.5
$O + H_2O \rightarrow HO^{\bullet} + HO^{\bullet}$	70.7	76.8	80.8	71.0
$O_2 + HOOH \rightarrow HO_2^{\bullet} + HO_2^{\bullet}$	161.1	178.2	182.2	181.7

[a] Experimental data from refs 35 and 36. [b] $\Delta H^{\ddagger} = E_a - 2RT - \Delta H_{assoc}$ at 298 K. [c] Estimated by use of the Marcus relation, eq 8, with $\Delta H_{int}^{\ddagger} = 20$ kJ mol^{-1}.

oxygen-atom centers, these range from very exothermic to very endothermic. The ΔH_{rxn} values are obtained from known heats of formation,[36] and the Arrhenius activation energies E_a are as tabulated in ref 35; the experimental enthalpies of activation at 298 K are now obtained as $\Delta H^{\ddagger} = E_a - 2RT - \Delta H_{assoc}$, where the latter term is the calculated enthalpy of association, as discussed above. It is assumed that the association energy of the product complex would be of similar magnitude to that for the reactant complex, and thus $\Delta H_{rxn} \approx (\Delta H_{rxn})^*$ in Figure 4. A value of $\Delta H_{int}^{\ddagger} = 20$ kJ mol^{-1} would lead to a root-mean-square error of less than 6 kJ mol^{-1} between predicted and experimental activation enthalpies, based upon the tabulated values of ΔH_{rxn}. However, since eq 8 is expected to be valid only for enthalpies of reaction of magnitude less than four times the intrinsic barrier,[34] a condition which is not satisfied by the data of Table 6, there may in retrospect be reason to doubt the significance of this Marcus-derived $\Delta H_{int}^{\ddagger} \approx 20 \pm 6$ kJ mol^{-1} in comparison with the calculated intrinsic barrier height discussed in the next section. Moreover, it is not obvious that the Marcus relation is applicable where, as in the present example, the intrinsic barrier has a large contribution from tunneling—a "nonsubstantial" effect.[17,38]

(iv) Ab Initio Barrier Heights. In Table 7 are shown total energies for the species involved in reaction 1, calculated by using the various methods employed in the G2 protocol. The barrier height obtained by G2 has not been corrected for the difference in vibrational zero point energy between the reactants and the transition state, which has a value of +1.67 kJ mol^{-1}, based on UMP2/6-31G* vibrational frequencies. The value for the barrier height of 41.5 kJ mol^{-1} obtained in G2 is actually in close agreement with the "best" estimate from our earlier study.[1] In the G2 protocol a basis correction calculated by the UMP4 method is added to the QCISD(T)/6-311G(d,p)//UMP2/6-31G(d) energy. It can be seen from the results in Table 7 that the effect of making this correction is to increase the barrier height from 38.2 to 41.5 kJ mol^{-1}. An important consideration in these calculations is the size of the BSSE, which results in the transition state being artificially lowered in energy relative to the separated reactants. If the completeness of the basis set is increased, which is what the G2 basis set correction does, the BSSE is reduced and consequently the energy of the transition state is increased. A close estimate of the BSSE at the QCISD(T)/6-311+G(3df,2p) level is provided by the value of 1.9 kJ mol^{-1} determined above for the HO$^{\bullet}$···HOH hydrogen-bonded adduct, which is the precursor complex to the transition structure. Two further observations can be made concerning the results in Table 7. First, using UMP2 instead of UMP4 to evaluate the basis set correction in the G2 protocol produces only a small difference in the resultant barrier heights. Second, the barrier height obtained by using QCISD(T)/6-311+G(3df,-2p) is almost identical to the G2 value. This finding adds support to the practice of calculating separately the effects of improvements in basis set and electron correlation.

Table 8 shows total energies and barrier heights from a series of calculations with the MRCISD method attempting to get agreement with the G2 barrier height. Two aspects of these calculations were varied to try and achieve more accurate results: the size of the basis set and the number of reference configurations. Three sets of MRCISD calculations using the 6-311++G(3d,2p) basis set were made, in which the number of CASSCF reference configurations was progressively increased. With a threshold value of 0.05 for the CASSCF configuration coefficient (five reference configurations for HOHOH$^{\bullet\ddagger}$), a barrier height of 80.9 kJ mol^{-1} was obtained. Note that the barrier height was found by taking the difference between the energy of the transition state and the energy of the two reactant molecules at a separation of 1000 Å, to avoid the problem of size inconsistency encountered in limited configuration interaction calculations.[24] Reduction of the threshold value to 0.01 (46 reference configurations for HOHOH$^{\bullet\ddagger}$), and then to 0.0005 (103 reference configurations for HOHOH$^{\bullet\ddagger}$), lowered the MRCISD barrier height to 57.8 kJ mol^{-1} and then to 54.5 kJ mol^{-1}. The final calculations involved 1 388 119 contracted (41 110 551 uncontracted) MRCISD configurations for HOHOH$^{\bullet\ddagger}$.

The barrier height obtained using full-valence CASSCF with the 6-311++G(3d,2p) basis set was 94.9 kJ mol^{-1}. This is the highest barrier obtained in this series of calculations; for comparison the barrier height found in our previous study with PUHF/6-311++G(3d,2p) was 117 kJ mol^{-1}. Nondynamical correlation energy—deriving from admixture of a small number of very important excited configurations—is therefore not of great importance in determining the barrier height for this reaction.

The downward trend in the MRCISD barrier heights produced by increasing the number of reference functions suggests that for a sufficiently large MRCISD calculation agreement might be obtained with the G2 value; but, interestingly, by applying the commonly used multireference equivalent of the Davidson correction[25] a consistent barrier height of 45−48 kJ mol^{-1} is obtained for all three MRCISD calculations. The QCISD(T) calculation in Table 8 using the same 6-311++G(3d,2p) basis set as for the MRCISD calculations gave a very similar barrier height of 44.5 kJ mol^{-1}. These results show that to obtain a converged ab initio value of the barrier height for a process such as reaction 1 a very good treatment of the dynamic correlation energy is required.

(v) Comparison with Experiment. Dubey et al. recently reported[37] rate constants for reaction 9 observed in the temperature range from 300 to 420 K, from which an Arrhenius activation energy of 17.6 ± 2 kJ mol^{-1} was obtained.

$$H^{18}O^{\bullet} + HOH \rightarrow H^{18}OH + {}^{\bullet}OH \qquad (9)$$

At 300 K the observed rate constant, $(2.2 \pm 1.0) \times 10^{-16}$ cm^3 molecule^{-1} s^{-1}, is greater than the VTST/SCSAG calculated value (Table 2) by a factor of more than 300, although it should

TABLE 7: Total Energies and Barrier Heights for the HO• + H_2O Symmetrical Hydrogen Atom Transfer Computed by Using Various Methods (Geometries Optimized with the UMP2/6-31G(d) Method)

	total energy, hartree			
method	H_2O	HO•	HOHOH•‡	barrier height, kJ mol^{-1}
QCISD(T)/6-311G(d,p)	−76.276 05	−75.589 21	−151.850 71	38.2
UMP2/6-311G(d,p)	−76.263 63	−75.572 76	−151.819 08	45.4
UMP2/6-311+G(3df,2p)	−76.318 10	−75.617 41	−151.916 26	50.5
PUMP2/6-311+G(3df,2p)	−76.318 10	−75.619 39	−151.924 48	34.2
UMP4/6-311+G(3df,2p)	−76.332 70	−75.635 95	−151.951 33	45.5
PUMP4/6-311+G(3df,2p)	−76.332 70	−75.637 09	−151.955 56	37.4
QCISD(T)/6-311+G(3df,2p)	−76.331 74	−75.636 80	−151.952 48	42.2
G2(MP2)	−76.330 51	−75.633 86	−151.947 89	43.3
G2	−76.332 70	−75.636 91	−151.953 81	41.5

TABLE 8: Total Energies and Barrier Heights for the HO• + H_2O Symmetrical Hydrogen Atom Transfer Computed by Using Various Methods (Geometries Optimized by the UMP2/6-311G(d,p) Method)

		total energy, hartree				barrier height, kJ mol^{-1}	
method	selection threshold for CASSCF configurations	H_2O	HO•	supermolecule (H_2O···HO•)	HOHOH•‡	reactants	molecule
CISD/6-311+G(d,p)		−76.271 84	−75.587 48	−151.842 22	−151.810 55	128.0	83.1
Davidson correction		−76.283 99	−75.595 67	−151.876 32	−151.853 64	68.3	59.5
CASSCF/6-311+G(d,p)		−76.106 05	−75.435 13	−151.541 18	−151.505 03	94.9	94.9
MRCISD/6-311+G(d,p)	0.01	−76.277 30	−75.590 03	−151.855 63	−151.833 85	87.9	57.2
Davidson correction	0.01	−76.284 46	−75.595 98	−151.878 49	−151.861 33	50.2	45.0
CASSCF/6-311++G(3d,2p)				−151.547 61	−151.511 17		95.7
MRCISD/6-311++G(3d,2p)	0.05			−151.894 24	−151.863 42		80.9
Davidson correction	0.05			−151.923 45	−151.905 04		48.3
MRCISD/6-311++G(3d,2p)	0.01			−151.895 80	−151.873 77		57.8
Davidson correction	0.01			−151.923 73	−151.906 66		44.8
MRCISD/6-311++G(3d,2p)	0.0005			−151.896 03	−151.875 28		54.5
Davidson correction	0.0005			−151.923 80	−151.906 62		45.1
QCISD(T)/6-311++G(3d,2p)		−76.311 67	−75.618 14		−151.912 86	44.5	

be borne in mind that these calculations are based upon the UMP2/6-311G(d,p) barrier height. A "best" theoretical estimate for the Arrhenius activation energy at 300 K may be obtained as follows. The VTST/SCSAG//UMP2/6-311G(d,p) calculated value of 22.5 kJ mol^{-1} (Table 3) is corrected by the difference (42.2−45.4 = −3.2 kJ mol^{-1}) between the UMP2/6-311G(d,p) and QCISD(T)/6-311+G(3df,2p) barrier heights (Table 7) and the estimated BSSE (+1.9 kJ mol^{-1}, Table 5) at the QCISD-(T)/6-311+G(3df,2p) level. This procedure yields a calculated value of 22.5 − 3.2 + 1.9 = 21.2 kJ mol^{-1} for the Arrhenius activation energy, which is a little higher than the experimental value of 17.6 ± 2 kJ mol^{-1}. We have already argued above, however, that application of the large-curvature method for tunneling could further reduce the calculated Arrhenius activation energy by up to 5 kJ mol^{-1} from the VTST/SCSAG estimate.

Conclusions

The conclusion of our earlier work, that the potential energy barrier height of the symmetric hydrogen atom exchange reaction (1) is about 41−45 kJ mol^{-1} with respect to separated reactants, has been confirmed by the more accurate calculations presented here. Agreement between the results of calculations using the G2 protocol and the multireference configuration interaction method was attained only after using the Davidson correction in MRCISD. The barrier height produced in the MRCISD calculations decreases slowly as the number of reference configurations is increased, and it may be concluded that the energy calculated for the transition state is very dependent on the quality of the treatment of dynamic correlation energy.

Our present calculations of the effect of tunneling using semiclassical transition state theory with the small-curvature approximation predict that the reduction in the activation energy is likely to be at least 20 kJ mol^{-1} for the symmetric reaction 1 at 300 K. Our best theoretical estimate for the Arrhenius activation energy, in the range 300−350 K, E_a = 21.2 kJ mol^{-1} with respect to separated reactants, is a little higher than the experimental value of 17.6 kJ mol^{-1} recently reported by Dubey et al.[37] for reaction 1 involving ^{18}O-labeled hydroxyl radical in the temperature range from 300 to 420 K. We consider that the remaining discrepancy is due to our use of the small-curvature tunneling correction. While a more precise evaluation of the tunneling correction, using the large-curvature method for the QCISD(T)/6-311+G(3df,2p) reaction surface, would be desirable, it is completely beyond the scope of the computational resources presently available to us.

A best theoretical estimate for the intrinsic barrier height $\Delta H_{int}^{\ddagger}$ may be obtained by subtracting the enthalpy of association of the hydrogen-bonded encounter complex HO•···HOH from the enthalpy of activation $\Delta H^{\ddagger}$ derived from the best theoretical estimate for E_a; i.e., $\Delta H_{int}^{\ddagger} = \Delta H^{\ddagger} - \Delta H_{assoc} = E_a - 2RT - \Delta H_{assoc}$ = 21.2−5.0 − (−8.9) = 25.1 kJ mol^{-1}. This estimate lies within the (rather wide) limits of uncertainty of the value 20 ± 6 kJ mol^{-1} derived above from a Marcus treatment of the activation energies and enthalpies of reaction for three nonsymmetric reactions.

Acknowledgment. We are grateful for financial support from the N.E.R.C. under the Atmospheric Chemistry Initiative and from the E.P.S.R.C. under the High Performance Computing Initiative; we also thank the E.P.S.R.C. for provision of computational facilities at the University of London Computer Centre. It is a pleasure to thank a referee for some very constructive comments, and we acknowledge correspondence with Professor Paul Marshall (University of North Texas).

References and Notes

(1) Francisco, J. S.; Williams, I. H. Atmospheric chemistry of organic halides. *The Chemistry of Functional Groups, Supplement D2: The Chemistry of Halides, Pseudo-Halides and Azides*; Patai, S., Rappoport, Z., Eds.; Wiley: Chichester, UK, 1995; Chapter 26, p 1559.

(2) Nanayakkara, A. A.; Balint-Kurti, G. G.; Williams, I. H. *J. Phys. Chem.* **1992**, *96*, 3662.

(3) Schlegel, H. B. *J. Chem Phys.* **1986**, *84*, 4530; **1988**, *92*, 3057.

(4) Pople, J. A.; Head-Gordon, M.; Raghavachari, K. *J. Chem. Phys.* **1987**, *87*, 5968.

(5) Boys, S. F.; Bernardi, F. *Mol. Phys.* **1970**, *19*, 533.

(6) Truong, T. N.; Truhlar, D. G. *J. Chem. Phys.* **1990**, *93*, 1761.

(7) Bell, R. P. *The Tunnel Effect in Chemistry*; Chapman and Hall: London, UK, 1980.

(8) Buchenau, H.; Toennies, J. P.; Arnold, J.; Wolfrum, J. *Ber. Bunsen-Ges. Phys. Chem.* **1990**, *94*, 1231.

(9) Smith, I. W. M. *Kinetics and Dynamics of Elementary Gas Reactions*: Butterworth: London, UK, 1980.

(10) Truhlar, D. G.; Garrett, B. C. *Annu. Rev. Phys. Chem.* **1984**, *35*, 159.

(11) Wigner, E. P. *Z. Phys. Chem.* **1932**, *B19*, 903.

(12) Eckart, C. *Phys. Rev.* **1930**, *35*, 1303.

(13) Marcus, R. A. *J. Chem. Phys.* **1965**, *43*, 1598.

(14) Levine, R. D.; Bernstein, R. B. *Molecular Reaction Dynamics and Chemical Reactivity*; Oxford University Press: Oxford, UK, 1987.

(15) Kupperman, A. Theory of Scattering: Papers in Honor of Henry Eyring. In *Theoretical Chemistry*; Vol. 6A, Henderson, D., Ed.; Academic: New York, 1981; Vol. 6A, p 80.

(16) Bondi, D. K.; Connor, J. N. L.; Garrett, B. C.; Truhlar, D. G. *J. Chem. Phys.* **1983**, *78*, 4931.

(17) Tucker, S. C.; Truhlar, D. G. In *New Theoretical Concepts for Understanding Organic Reactions*; Bertran, J., Csizmadia, I., Eds.; NATO ASI Series C, 267; Kluwer: Dordrecht, Netherlands, 1989; p 291.

(18) Steinfeld, J. I.; Francisco, J. S.; Hase, W. L. *Chemical Kinetics and Dynamics*; Prentice Hall: Englewood Cliffs, NJ, 1989.

(19) Curtiss, L. A.; Raghavachari, K.; Trucks, G. W.; Pople, J. A. *J. Chem. Phys.* **1991**, *94*, 7221.

(20) Lu, D.-H.; Truong, T. N.; Melissas, V. S.; Lynch, G. C.; Liu, Y.-P.; Garrett, B. C.; Steckler, R.; Isaacson, A. D.; Rai, S. N.; Hancock, G. C.; Lauderdale, J. G.; Joseph, T.; Truhlar, D. G. *Comput. Phys. Commun.* **1992**, *71*, 235. Liu, Y.-P.; Lynch, G. C.; Hu, W.-P.; Melissas, V. S.; Steckler, R.; Garrett, B. C.; Lu, D.-H.; Truong, T. N.; Isaacson, A. D.; Rai, S. N.; Hancock, G. C.; Lauderdale, J. G.; Joseph, T.; Truhlar, D. G. *POLYRATE*, QCPE program 601-version 5.0.1, Quantum Chemistry Program Exchange, Indiana University, Bloomington, IN, 1993; *QCPE Bull.* **1993**, *13*, 28.

(21) Gonzalez, C.; Schlegel, H. B. *J. Chem. Phys.* **1989**, *90*, 2154; *J. Phys. Chem.* **1990**, *94*, 5523.

(22) *GAUSSIAN 92*, Revision A, Frisch, M. J.; Trucks, G. W.; Head-Gordon, M.; Gill, P. M. W.; Wong, M. W.; Foresman, J. B.; Johnson, B. G.; Schlegel, H. B.; Robb, M. A.; Replogle, E. S.; Gomperts, R.; Andres, J. L.; Raghavachari, K.; Binkley, J. S.; Gonzalez, C.; Martin, R. L.; Fox, D. J.; Defrees, D. J.; Baker, J.; Stewart, J. J. P.; Pople, J. A. Gaussian, Inc., Pittsburgh, PA, 1992.

(23) *MOLPRO*, a package of ab initio programs written by Werner, H.-J.; Knowles, P. J. (with contributions by Almlof, J.; Amos, R.; Elbert, S.; Hampel, K.; Meyer, W.; Peterson, K.; Pitzer, R.; Stone, A.); Werner, H.-J.; Knowles, P. J. *J. Chem. Phys.* **1985**, *82*, 5053. Knowles, P. J.; Werner, H.-J. *Chem. Phys. Lett.* **1985**, *115*, 259. Werner, H.-J.; Knowles, P. J. *J. Chem. Phys.* **1988**, *89*, 5803. Knowles, P. J.; Werner, H.-J. *Chem. Phys. Lett.* **1988**, *145*, 514.

(24) Meyer, W. *J. Chem. Phys.* **1973**, *58*, 1017.

(25) Langhoff, S. R.; Davidson, E. R. *Int. J. Quantum Chem.* **1974**, *8*, 61.

(26) Durant, J. L.; McMichael Rohlfing, C. *J. Chem. Phys.* **1993**, *98*, 8031.

(27) Frisch, M. J.; Trucks, G. W.; Schlegel, H. B.; Gill, P. M. W.; Johnson, B. G.; Robb, M. A.; Cheeseman, J. R.; Keith, T.; Petersson, G. A.; Montgomery, J. A.; Raghavachari, K.; Al-Laham, M. A.; Zakrzewski, V. G.; Ortiz, J. V.; Foresman, J. B.; Peng, C. Y.; Ayala, P. Y.; Chen, W.; Wong, M. W.; Andres, J. L.; Repogle, E. S.; Gomperts, R.; Martin, R. L.; Fox, D. J.; Binkley, J. S.; Defrees, D. J.; Baker, J.; Stewart, J. J. P.; Head-Gordon, M.; Gonzalez, C.; Pople, J. A. Gaussian 94, Revision B.3, Gaussian, Inc., Pittsburgh, PA, 1995.

(28) Fox, G. L.; Schlegel, H. B. *J. Am. Chem. Soc*. **1993**, *115*, 6870.

(29) Hu, W.-P.; Liu, Y.-P.; Truhlar, D. G. *J. Chem. Soc., Faraday Trans.* **1994**, *90*, 1715.

(30) Xie, Y.-M.; Schaefer, H. F. *J. Chem. Phys.* **1993**, *98*, 8829.

(31) Kim, K. S.; Kim, H. S.; Jang, J. H.; Kim, H. S.; Mhin, B.-J.; Xie, Y.-M.; Schaefer, H. F. *J. Chem. Phys.* **1991**, *94*, 2057.

(32) Curtiss, L. A.; Raghavachari, K.; Pople, J. A. *J. Chem. Phys.* **1993**, *98*, 1293.

(33) van Duijneveldt, F. B.; van Duijneveldt-van de Rijdt, J. G. C. M.; van Lenthe, J. H. *Chem. Rev.* **1994**, *94*, 1873.

(34) Marcus, R. A. *J. Phys. Chem.* **1968**, *72*, 891.

(35) Westbrook, C. K.; Dryer, F. L. *Combust. Sci. Technol.* **1979**, *20*, 125.

(36) *JANAF Thermochemical Tables*, 3rd ed.; Chase, M. W.; Davies, C. A.; Downey, J. R.; Frurip, D. J.; McDonald, R. A.; Syverud, A. N. *J. Phys. Chem. Ref. Data Suppl. No. 1* **1985**, *14*.

(37) Dubey, M. K.; Mohrschladt, R.; Donahue, N. M.; Anderson, J. G. *J. Phys. Chem. A* **1997**, *101*, 1494.

(38) Truhlar, D. G.; Garrett, B. C. *J. Am.Chem. Soc*. **1989**, *111*, 1232.